

Intertwined Charge and Spin Density Waves in Trilayer Nickelate $\text{La}_4\text{Ni}_3\text{O}_{10}$ Revealed by ^{139}La NQR

Jie Dou,^{1,2,*} Feiyu Li,^{3,*} Mingxin Zhang,^{4,*} Jun Luo,¹ Shuo Li,¹ Aifang Fang,^{5,6} Jie Yang,¹ Yanpeng Qi,^{4,7,8,†} Junjie Zhang,^{3,‡} and Rui Zhou^{1,2,§}

¹*Institute of Physics, Chinese Academy of Sciences,*

and Beijing National Laboratory for Condensed Matter Physics, Beijing 100190, China

²*School of Physical Sciences, University of Chinese Academy of Sciences, Beijing 100190, China*

³*State Key Laboratory of Crystal Materials, Institute of Crystal Materials,
Shandong University, Jinan, Shandong 250100, China*

⁴*State Key Laboratory of Quantum Functional Materials,
School of Physical Science and Technology,
ShanghaiTech University, Shanghai 201210, China*

⁵*School of Physics and Astronomy, Beijing Normal University, Beijing 100875, China*

⁶*Key Laboratory of Multiscale Spin Physics, Ministry of Education,
Beijing Normal University, Beijing 100875, China*

⁷*ShanghaiTech Laboratory for Topological Physics,
ShanghaiTech University, Shanghai 201210, China*

⁸*Shanghai Key Laboratory of High-resolution Electron Microscopy,
ShanghaiTech University, Shanghai 201210, China*

(Dated: January 27, 2026)

Abstract

The discovery of superconducting transitions in pressurized $\text{La}_3\text{Ni}_2\text{O}_7$ and $\text{La}_4\text{Ni}_3\text{O}_{10}$ has highlighted the pivotal role of density wave (DW) orders in nickelate superconductors. To gain a comprehensive understanding of the superconducting state, it is essential to elucidate the nature of the DW order. In this study, we utilized ^{139}La nuclear quadrupole resonance (NQR) to investigate the charge density wave (CDW) and spin density wave (SDW) orders in both single-crystal and polycrystalline $\text{La}_4\text{Ni}_3\text{O}_{10}$. Near $T_{\text{DW}} \approx 133$ K, an abrupt change in both the linewidth and frequency of the La(2) site in the single-crystal sample provides compelling evidence for a first-order-like phase transition. The pronounced broadening of the NQR lines indicates the incommensurate nature of the DW order. Furthermore, the spin-lattice relaxation rate divided by temperature $1/T_1 T$ exhibits a strong enhancement at T_{DW} , indicating the strong spin fluctuations above the first-order DW transition. These observations suggest an intricate interplay between incommensurate CDW and SDW orders. Our findings offer critical insights into the microscopic mechanisms of the DW state in $\text{La}_4\text{Ni}_3\text{O}_{10}$ and establish an essential framework for exploring the interplay between DW and superconducting phases in nickelate superconductors.

^{*}These authors contributed equally to this work.

[†]Electronic address: qiyp@shanghaitech.edu.cn

[‡]Electronic address: junjie@sdu.edu.cn

[§]Electronic address: rzhou@iphy.ac.cn

I. INTRODUCTION

The recent discovery of superconductivity in nickelates, particularly the breakthrough in pressurized Ruddlesden-Popper (RP) phase $\text{La}_3\text{Ni}_2\text{O}_7$ [1–3] and $\text{La}_4\text{Ni}_3\text{O}_{10}$ [4–7], has presented a new opportunity for studying the superconducting pairing mechanism of high- T_c superconductors. Although RP-phase nickelates are non-superconducting at ambient pressure, magnetic orders were observed in different nickelates[8–15] – a feature shared with both cuprate[16] and iron-based superconductors[17]. Therefore, understanding the emergence of magnetic ordered states is of great significance for understanding superconductivity[18–22]. Among various nickelates, $\text{La}_4\text{Ni}_3\text{O}_{10}$ has attracted significant attention due to its high superconducting volume fraction[4], well-defined interlayer stacking ordering and intertwined charge- and spin-density wave (DW) orders[23]. These characteristics not only make $\text{La}_4\text{Ni}_3\text{O}_{10}$ an important platform for investigating DW orders but also facilitate the exploration of the microscopic origin of unconventional superconductivity.

At ambient pressure, $\text{La}_4\text{Ni}_3\text{O}_{10}$ crystallizes in the monoclinic $\text{P}2_1/\text{a}$ space group (Fig. 1(a))[4], with NiO_6 octahedra tilted away from the c -axis. Early electrical and magnetic transport studies[8–10] have provided evidence for the potential emergence of DW orders in $\text{La}_4\text{Ni}_3\text{O}_{10}$ near 140 K. Subsequently, through low-temperature X-ray diffraction (XRD) and neutron scattering experiments on single crystals, both charge- and spin-density wave orders have been observed in $\text{La}_4\text{Ni}_3\text{O}_{10}$ [23]. Under high pressures, the suppression of the DW order and the emergence of the superconducting phase occur nearly simultaneously in the vicinity of the structural transition[4], suggesting a potential competitive interplay among these electronic orders. Later, various microscopic techniques have been utilized to obtain more microscopic information regarding the DW state. Ultrafast spectroscopy has uncovered a weaker correlation in $\text{La}_4\text{Ni}_3\text{O}_{10}$ compared to that in the bilayer nickelate $\text{La}_3\text{Ni}_2\text{O}_7$ [24, 25]. Nevertheless, the DW order still strongly competes with superconductivity [26]. Scanning tunneling microscopy (STM) measurements[27] have uncovered an incommensurate unidirectional CDW in $\text{La}_4\text{Ni}_3\text{O}_{10}$, which is consistent with previous XRD findings[23]. Recent muon spin relaxation (μSR) measurements[28, 29] suggest that the SDW order is also incommensurate, which seems to be consistent with previous neutron scattering measurements[23]. Nevertheless, a second SDW order was observed in polycrystalline samples by μSR measurements[28, 29], and this has not been observed in any other measurements to date. Simultaneously, the question of whether the DW orders are predominantly governed by charge,

spin, or an intertwined order remains unresolved, and their origin and microscopic mechanisms necessitate systematic investigation. Thus, a local probe is of crucial importance for clarifying the microscopic mechanisms underlying DW orders.

The nuclear quadrupole resonance (NQR) exhibits high sensitivity to local electric field gradients (EFG) and internal magnetic fields associated with CDW and SDW formations. Owing to the use of polycrystalline samples and limitations in sample quality, previous nuclear magnetic resonance (NMR) and NQR studies[30, 31] on $\text{La}_4\text{Ni}_3\text{O}_{10}$ have not provided detailed spectroscopic information regarding the DW transition, particularly concerning SDW order and related magnetic fluctuations. In this article, we utilize $^{139}\text{La}(2)$ NQR to explore DW orders in polycrystalline and single-crystal $\text{La}_4\text{Ni}_3\text{O}_{10}$ under ambient pressure. Below $T_{\text{DW}} \approx 133$ K, the sudden broadening of the linewidth and frequency shifts, particularly in the $\pm 5/2 \leftrightarrow \pm 7/2$ transition, reveal a first-order-like DW transition. The significant broadening of the NQR lines suggests the incommensurate nature of the DW order. Moreover, the temperature-dependent spin-lattice relaxation rate $1/T_1T$ shows a notable enhancement at T_{DW} , suggesting the onset of strong spin fluctuations above the first-order DW transition. These findings imply that the first-order transition is likely induced by the CDW, while the spin fluctuations stem from the SDW, indicating a complex interplay between incommensurate CDW and SDW orders. These results not only elucidate the microscopic mechanisms underlying the DW state in $\text{La}_4\text{Ni}_3\text{O}_{10}$ but also establish a crucial framework for investigating the interaction between DW and superconducting phases in nickel-based superconductors.

II. NQR METHODS

The polycrystalline and single-crystal samples of $\text{La}_4\text{Ni}_3\text{O}_{10}$ were synthesized via the sol-gel method [32] and flux growth method [33], respectively. The ^{139}La NQR spectra were acquired by sweeping the frequency point by point and integrating the spin-echo intensity in the absence of any applied static magnetic fields. The amounts of the polycrystalline and single-crystal samples employed for NQR measurement were approximately 600 mg and 80 mg, respectively. Given that the principal axis of ^{139}La is aligned along the c -axis, the single-crystal samples were oriented along the c -axis, which could ensure that the radio frequency field H_1 was within the ab plane. This enabled us to use a much smaller coil for NQR measurements on single crystal samples as compared to polycrystalline samples. During NQR experiments, a much larger ringing signal of

the polycrystalline sample was observed at low frequencies. As a result, an interval of $\tau = 120 \mu\text{s}$ between the $\pi/2$ and π pulses was used for the polycrystalline samples at low frequencies, while only an interval of $50 \mu\text{s}$ was used for single crystal samples. The use of a longer τ will lead to the loss of the NQR signal at low frequencies for polycrystalline samples. The spin-lattice relaxation time T_1 was measured using the saturation-recovery method. The spin-lattice relaxation time T_1 and the stretched-exponential factor β are achieved by fitting the relaxation curves via the stretched exponential formula[34]: $(M_0 - M(t))/M_0 = \frac{3}{22}e^{-21(\frac{t}{T_1})^\beta} + \frac{50}{77}e^{-10(\frac{t}{T_1})^\beta} + \frac{3}{14}e^{-3(\frac{t}{T_1})^\beta}$. Because η is close to zero, we ignore the influence of η on the recovery curve.

III. RESULTS AND DISCUSSIONS

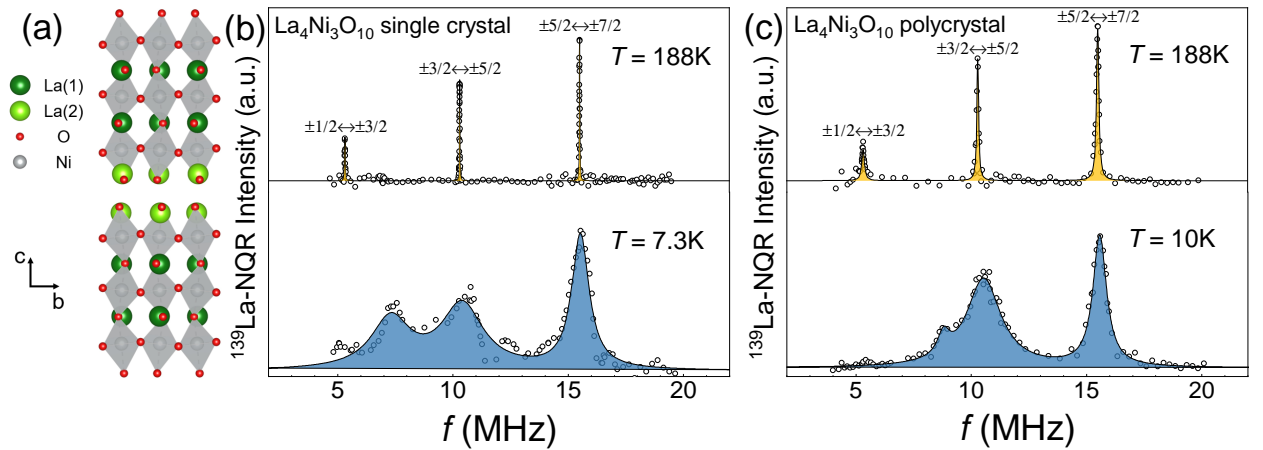


FIG. 1: (a) Crystal structure of $\text{La}_4\text{Ni}_3\text{O}_{10}$. Light green atoms denote La(2) atoms, while dark green atoms denote La(1) atoms. (b-c) The ^{139}La NQR spectra of $\text{La}_4\text{Ni}_3\text{O}_{10}$ single-crystal (b) and polycrystalline (c) samples in the normal state and the DW state, respectively. The yellow and blue peaks correspond to the signals of $\text{La}_4\text{Ni}_3\text{O}_{10}$ before and after the transition, respectively. All lines are fitted using Lorentz functions, which serve as visual guides.

La atoms occupy two distinct crystallographic sites as shown in Fig. 1(a). Specifically, La(1) is positioned within the NiO_2 bilayers, while La(2) is located outside the NiO_2 trilayers. The quadrupole frequency is defined as $\nu_q = \frac{3e^2qQ}{2I(2I-1)h}$, where eq represents the EFG, Q is the nuclear quadrupole moment, I denotes the nuclear spin quantum number, and h is the Planck's constant. For the ^{139}La nucleus with a spin of $7/2$, the NQR spectrum is expected to exhibit three resonance lines corresponding to the $\pm 1/2 \leftrightarrow \pm 3/2$, $\pm 3/2 \leftrightarrow \pm 5/2$, and $\pm 5/2 \leftrightarrow \pm 7/2$ transitions. Thus, a total

of six lines are anticipated to be observable in the ^{139}La NQR spectrum of $\text{La}_4\text{Ni}_3\text{O}_{10}$. However, the La(1) site exhibits a significantly lower v_q (2.2 MHz) and a longer T_1 [30, 31] compared to that of the La(2) site. As a result, at 188 K, only three characteristic NQR lines from the La(2) sites are observed in single-crystal and polycrystalline samples, respectively (see Fig. 1(b) and 1(c), top panels). Compared with the $\text{La}_4\text{Ni}_3\text{O}_{10}$ polycrystalline samples, the NQR linewidth of the single crystal samples is much smaller at 188 K, indicating that the single-crystal samples have better crystal quality. In other words, the single-crystal samples contain fewer disorders or oxygen vacancies.

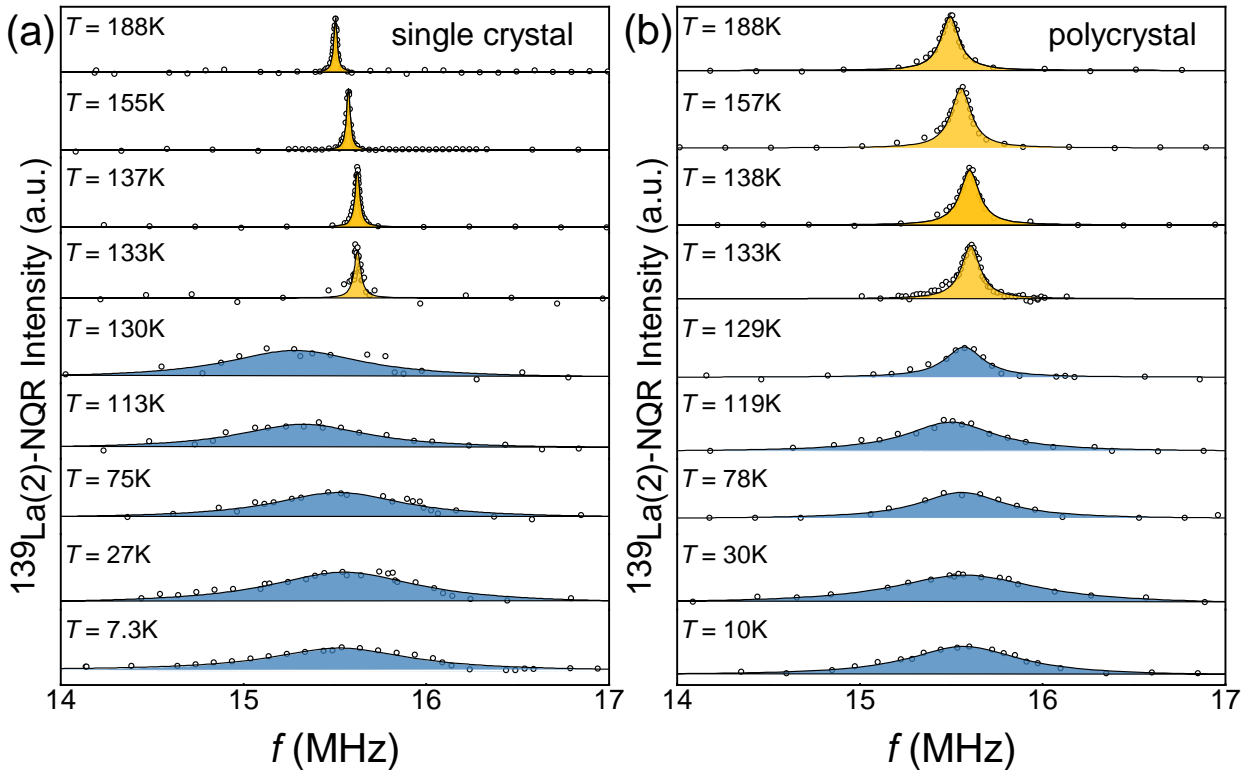


FIG. 2: The temperature-dependent $^{139}\text{La}(2)$ NQR spectra of $\text{La}_4\text{Ni}_3\text{O}_{10}$ single-crystal (a) and polycrystal (b) samples. The yellow and blue peaks represent the $\pm 5/2 \leftrightarrow \pm 7/2$ transition lines of $\text{La}_4\text{Ni}_3\text{O}_{10}$ before and after the DW transition, respectively. The solid lines represent the Lorentz fit.

As the temperature decreases far below the DW transition temperature T_{DW} , a notable line broadening is observed in both single-crystal and polycrystal samples (see Fig. 1(b) and 1(c), bottom panels). For both types of samples, only one broad line is observable around the two NQR lines corresponding to the $\pm 5/2 \leftrightarrow \pm 7/2$ and $\pm 3/2 \leftrightarrow \pm 5/2$ transitions. Nevertheless, in the case of single-crystal samples, an additional broad line is seen at lower frequencies. This could be

attributed to the fact that a much smaller interval τ between $\pi/2$ and π pulses can be employed for NQR measurements of single-crystal samples. The use of a much longer τ , resulting from the emergence of a larger ringing signal, can cause the loss of the NQR signal at low frequencies in polycrystalline samples.

Figure 2 further shows the temperature dependence of the NQR lines corresponding to the $\pm 5/2 \leftrightarrow \pm 7/2$ transition for both single crystal and polycrystalline samples, respectively. Although a clear broadening appears below T_{DW} for both types of samples, the temperature-dependent behaviors just below T_{DW} are not identical. In the case of single-crystal samples, the line broadening and shift at the $\pm 5/2 \leftrightarrow \pm 7/2$ transition occur abruptly below the DW transition temperature $T_{DW} \approx 133$ K (as shown in Fig. 2(a)). However, for polycrystalline samples below $T_{DW} \approx 133$ K, a gradual change in linewidth and frequency is observed. Figure 3 summarizes the temperature dependence of the frequency and full width at half maximum (FWHM) of the NQR line corresponding to the $\pm 5/2 \leftrightarrow \pm 7/2$ transition. It is readily apparent that the DW transition in the single-crystal sample exhibits characteristics reminiscent of a first-order transition. Considering the better quality of single crystal samples, the more abrupt change below T_{DW} is more likely associated with the intrinsic characteristics of $\text{La}_4\text{Ni}_3\text{O}_{10}$. A greater degree of disorder or a larger distribution of oxygen vacancies in the sample would render the transformation more gradual. Similar behavior was observed through specific heat measurements, where a smaller jump of the specific heat at the transition was seen in polycrystalline samples[29]. Our observation in $\text{La}_4\text{Ni}_3\text{O}_{10}$ differs from previous NQR results in $\text{La}_3\text{Ni}_2\text{O}_7$, where the DW phase transition was identified as second-order[15]. Especially, we note that previous μSR studies on single-crystal samples indicated a second-order phase transition[12], suggesting that $\text{La}_3\text{Ni}_2\text{O}_7$ and $\text{La}_4\text{Ni}_3\text{O}_{10}$ likely display distinct behaviors. However, earlier NQR studies used polycrystalline samples[30, 31], and the spectra near the transition may resemble those of polycrystalline $\text{La}_4\text{Ni}_3\text{O}_{10}$, which are influenced by sample quality. To conclusively determine the nature of the transition, it would be essential to conduct similar NQR measurements on high-quality single-crystal samples in the future. Additionally, for both single crystal and polycrystal samples, no abrupt increases in FWHM was observed below $T \approx 90$ K, at which a second SDW transition was observed by recent μSR measurements[28, 29]. Given that the La(2) site is only sensitive to the magnetic moments of the outer NiO_2 planes, it is plausible that the change observed by μSR measurements is associated with the inner NiO_2 planes. Further NMR studies on the La(1) site are necessary to clarify this issue.

Next we discuss the origin of the changes in the NQR spectra in the DW state. Firstly, unlike

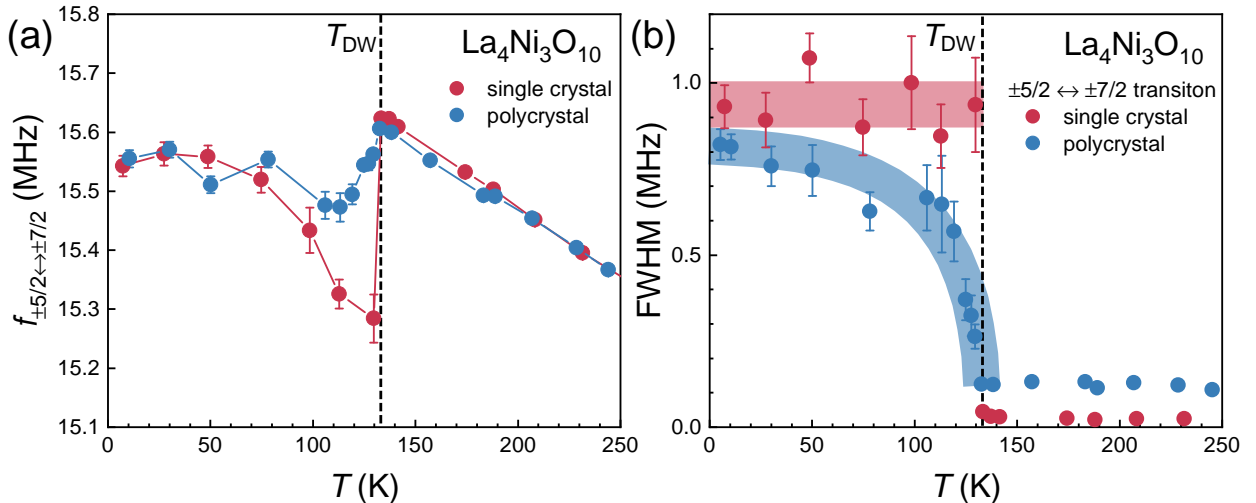


FIG. 3: The temperature-dependent NQR frequency (a) and full width at half maximum(FWHM) (b) of the line corresponding to the $\pm 5/2 \leftrightarrow \pm 7/2$ transition in single-crystal(red dots) and polycrystal(blue dots) $\text{La}_4\text{Ni}_3\text{O}_{10}$. Both of them start to increase below $T_{\text{DW}} \approx 133$ K marked by the dashed line. The error bar is the s.d. in fitting spectra by the Lorentz function.

$\text{La}_3\text{Ni}_2\text{O}_7$, we did not observe splitting on each NQR line, especially the NQR line corresponding to the $\pm 5/2 \leftrightarrow \pm 7/2$ transition[15]. This indicates that the DW order in this sample is incommensurate and different from that of $\text{La}_3\text{Ni}_2\text{O}_7$. In this case, it would only cause broadening of the NQR spectrum. Meanwhile, we did not observe the double-horn structure of one-dimensional incommensurate peaks[35], indicating that the incommensurate modulation is most likely to be two-dimensional. In principle, the broadening of the NQR spectra arises from two distinct contributions: one is due to changes in the local EFG caused by charge modulation, and the other originates from the formation of an internal magnetic field B_{int} . If the internal magnetic field at the La(2) site aligns along the c -axis, both the $\pm 3/2 \leftrightarrow \pm 5/2$ and $\pm 5/2 \leftrightarrow \pm 7/2$ transitions would shift and broaden identically[15]. However, the broadening of the NQR lines corresponding to the $\pm 1/2 \leftrightarrow \pm 3/2$ and $\pm 3/2 \leftrightarrow \pm 5/2$ transitions are significantly larger than that of the $\pm 5/2 \leftrightarrow \pm 7/2$ transition in both single-crystal and polycrystalline samples at low temperatures (see Fig. 1(b) and 1(c), bottom panels). Meanwhile the two low frequency lines also shift to higher frequencies. If the internal magnetic field at the La(2) site aligns perpendicular to the c -axis, the NQR lines corresponding to the $\pm 1/2 \leftrightarrow \pm 3/2$ and $\pm 3/2 \leftrightarrow \pm 5/2$ transitions should shift to higher frequencies and broaden a lot as indicated by previous NQR calculations[15]. This seems to in agreement with our experimental results. However, in this case, the internal magnetic field would barely affect the

NQR line corresponding to the $\pm 5/2 \leftrightarrow \pm 7/2$ transition, which can not explain the large increase of linewidth of this NQR line. Besides this, we also note that the change of NQR lines cannot be solely attributed to quadrupole broadening caused by charge modulation too. In the case of quadrupole broadening, one would expect the broadening of each NQR lines is proportional to the NQR frequencies[15], which is also inconsistent with our observation. Taken all together, our results implies that the change of the NQR spectra is not related to only one kind of DW. Instead, both charge and spin density waves develop below T_{DW} , which is consistent with previous neutron scattering studies[23].

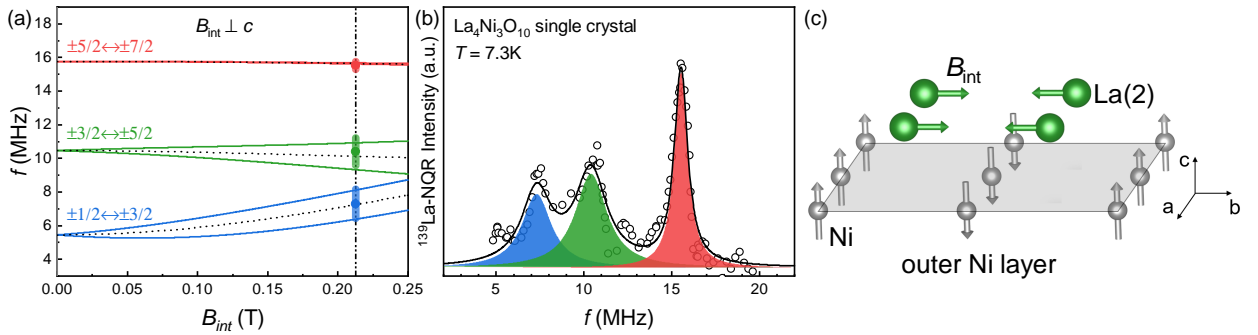


FIG. 4: (a) Theoretical simulation of the NQR frequencies at the La(2) site with an internal magnetic field perpendicular to the c -axis. The red, green, and blue curves represent the field-dependent shifts of the $\pm 5/2 \leftrightarrow \pm 7/2$, $\pm 3/2 \leftrightarrow \pm 5/2$ and $\pm 1/2 \leftrightarrow \pm 3/2$ transitions, respectively. If the SDW order is commensurate, distinct line splitting should be discerned for NQR lines corresponding to the $\pm 5/2 \leftrightarrow \pm 7/2$ and $\pm 3/2 \leftrightarrow \pm 5/2$ transitions. Nevertheless, in the DW state, only broad lines are observed owing to the incommensurate spin and charge modulation. The black dashed line depicts their average frequencies in the DW state. Solid circles represent the frequencies of three NQR lines derived from the experimental results presented in panel (b). The color bars represent the FWHM contributed by the internal magnetic field, which is proportional to the splitting of NQR lines due to SDW. (b) Spectrum of $\text{La}_4\text{Ni}_3\text{O}_{10}$ single crystal at 7.3 K. The solid lines denote Lorentz fits. The resolved three peaks correspond to the $\pm 5/2 \leftrightarrow \pm 7/2$ (red), $\pm 3/2 \leftrightarrow \pm 5/2$ (green) and $\pm 1/2 \leftrightarrow \pm 3/2$ (blue) transitions. The ν_q and η are taken as 5.27 MHz and 0.1 for the calculation, respectively. (c) Schematic diagram of the internal magnetic field at the La(2) site within $\text{La}_4\text{Ni}_3\text{O}_{10}$. The grey and green arrows represent the Ni magnetic moments and the internal magnetic field B_{int} , respectively.

As we noted that the two NQR lines corresponding to $\pm 1/2 \leftrightarrow \pm 3/2$ and $\pm 3/2 \leftrightarrow \pm 5/2$ exhibit a clear shift towards higher frequencies in Fig. 4(b), we assume that an internal magnetic field B_{int} at the La(2) site is perpendicular to the c -axis. To simulate the experimentally obtained NQR

spectrum, as shown in Fig. 4(a), we assume that the broadening caused by charge modulations is W_{CDW} . In the DW state, the spectrum is broadened nearly symmetrically and follows a Lorentzian distribution. Since the FWHM of the convolution of two Lorentzian functions is the sum of their individual FWHM, the total broadening of each NQR spectrum can be considered to consist of two components: $W^i = W_{\text{CDW}}^{i \leftrightarrow (i+1)} + W_{\text{SDW}}^{i \leftrightarrow (i+1)}$ ($i = 1/2, 3/2, 5/2$). Among these, $W_{\text{CDW}}^{i \leftrightarrow (i+1)}$ is proportional to the frequency of the NQR line, such that $W_{\text{CDW}}^{1/2 \leftrightarrow 3/2} : W_{\text{CDW}}^{3/2 \leftrightarrow 5/2} : W_{\text{CDW}}^{5/2 \leftrightarrow 7/2} = 1:2:3$. $W_{\text{SDW}}^{i \leftrightarrow (i+1)}$ is proportional to the splitting of the NQR spectrum induced by the internal magnetic field B_{int} . The shift of the NQR spectrum can also be attributed to B_{int} . As shown in Fig. 4(a), we found that when $B_{\text{int}} \sim 210$ mT and $W_{\text{CDW}}^{1/2} = 0.3$ MHz, both the shift and broadening of the NQR spectrum are consistent with the experimental results. Our simulation results also suggest, the pronounced NQR line shift and broadening in $\text{La}_4\text{Ni}_3\text{O}_{10}$ in the DW state originate from collective modulation by incommensurate CDW and SDW orders. We further note that the internal magnetic field arising from the magnetic moment of Ni is significantly larger than that in $\text{La}_3\text{Ni}_2\text{O}_7$ ($B_{\text{int}} \sim 5$ mT)[15]. Our results suggest that the magnetic moment of Ni on the outer planes is much larger in $\text{La}_4\text{Ni}_3\text{O}_{10}$ than that in $\text{La}_3\text{Ni}_2\text{O}_7$ [15]. Moreover, we note that previous neutron scattering experiments have indicated a stripe-type antiferromagnetic order[23]. Regarding the orientation of the Ni magnetic moments, one possibility is that they lie within the *ab*-plane, as observed in Fe-based superconductors[17]. However, due to coupling with the four neighboring Ni moments, this would result in an internal magnetic field at the La(2) site aligned along the *c*-axis[36], which is inconsistent with our experimental observations. Alternatively, as proposed by a prior theoretical study[22] (see Fig. 4(c)), the Ni magnetic moments on the outer Ni layer may be oriented along the *c*-axis. In this case, the internal magnetic field at the La(2) site in $\text{La}_4\text{Ni}_3\text{O}_{10}$ would be perpendicular to the *c*-axis, in agreement with our simulation results (Fig. 4(c)). Thus, our findings support the interpretation that the Ni magnetic moments on the outer layer are aligned along the *c*-axis in $\text{La}_4\text{Ni}_3\text{O}_{10}$, which is similar to the observation in $\text{La}_3\text{Ni}_2\text{O}_7$ [14].

We further investigated the DW transition through spin-lattice relaxation rate measurements. Similar to the case of $\text{La}_3\text{Ni}_2\text{O}_7$ [15], a pronounced peak is observed in the temperature-dependent $1/T_1T$ at the transition temperature T_{DW} for the single-crystal sample as shown in Fig. 5. For both $\text{La}_3\text{Ni}_2\text{O}_7$ and $\text{La}_4\text{Ni}_3\text{O}_{10}$, the stretched-exponential factor β decreases rapidly below T_{DW} shown in Fig. 5(c), resulting from the spin and charge modulation in the DW order. In comparison with the single-crystal samples, the polycrystal samples exhibit a much weaker enhancement, further highlighting the superior quality of the single-crystal samples. Similar to $\text{La}_3\text{Ni}_2\text{O}_7$, the strong

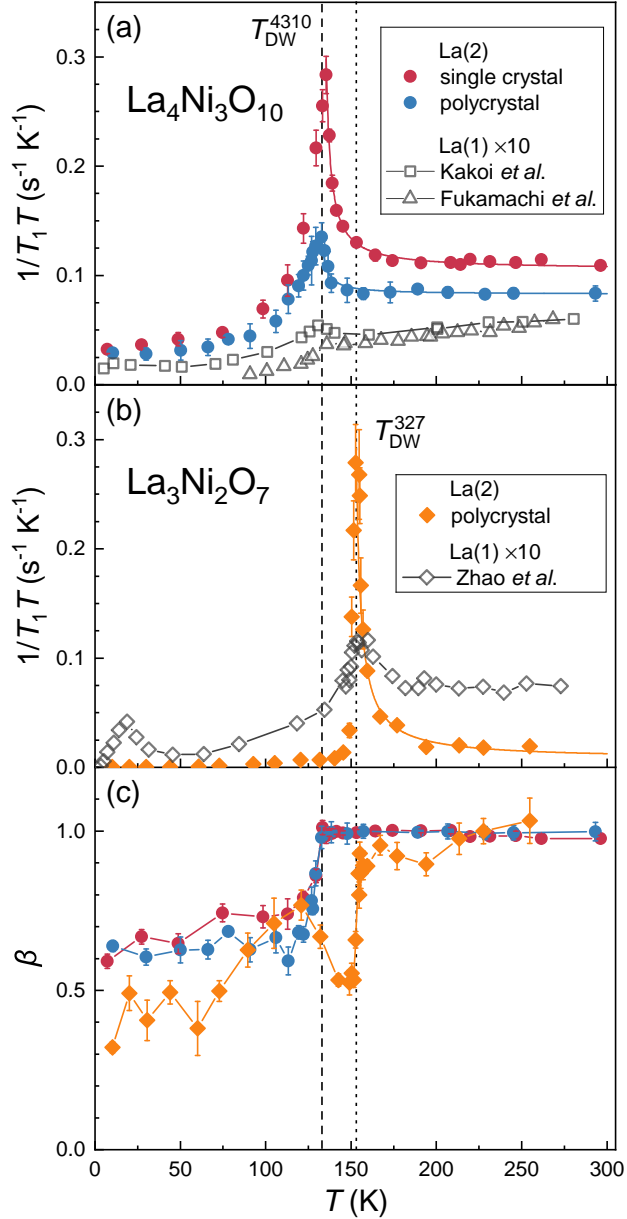


FIG. 5: (a) Red dots and blue symbols represent the $1/T_1T$ measured at the La(2) site in $\text{La}_4\text{Ni}_3\text{O}_{10}$ single crystal and polycrystal, respectively. Grey squares and triangles represent the $1/T_1T$ measured at the La(1) site reported by T. Fukamachi et al.[30] and M. Kakoi et al.[31], respectively. (b) Orange and grey diamonds represent the $1/T_1T$ measured at the La(2) and La(1) sites by J. Luo et al.[15] and D. Zhao et al.[14], respectively. (c) Temperature dependence of the β of $\text{La}_3\text{Ni}_2\text{O}_7$ (orange diamonds)[15], $\text{La}_4\text{Ni}_3\text{O}_{10}$ single crystal (red circles) and polycrystal (blue circles). The error bars of $1/T_1T$ and β are the s.d. in fitting the recovery curve. The dashed and dotted lines represent T_{DW} in $\text{La}_4\text{Ni}_3\text{O}_{10}$ and $\text{La}_3\text{Ni}_2\text{O}_7$, respectively. Note that all the $1/T_1T$ values for the La(1) site have been scaled by a factor of 10.

enhancement of $1/T_1T$ is most likely attributable to spin fluctuations. However, considering that the DW transition in $\text{La}_4\text{Ni}_3\text{O}_{10}$ is of the first order, spin fluctuations associated with the DW order are expected to be negligible above T_{DW} . In $\text{La}_3\text{Ni}_2\text{O}_7$, where the transition is second order, such fluctuations are naturally more prominent. The nearly identical enhancement of $1/T_1T$ in $\text{La}_4\text{Ni}_3\text{O}_{10}$, despite its first-order transition nature, appears contradictory. A plausible explanation is that the first-order transition is driven by the charge density wave[37], while the strong enhancement of $1/T_1T$ originates from spin fluctuations, akin to what has been observed in the kagome metal CsV_3Sb_5 [38, 39]. Additionally, we note that the temperature-dependent $1/T_1T$ results reported by M. Kakoi et al. (Fig. 5(a))[30] exhibit only a minor peak. This relatively small enhancement of $1/T_1T$ at T_{DW} may be attributed to sample quality. In particular, T. Fukamachi et al. observed no peak in the temperature dependence of $1/T_1T$ at T_{DW} [31]. However, it is also noteworthy that in $\text{La}_3\text{Ni}_2\text{O}_7$, the enhancement of $1/T_1T$ at the La(1) site is indeed much smaller than that at the La(2) site (Fig. 5(b)). Moreover, in both $\text{La}_3\text{Ni}_2\text{O}_7$ and $\text{La}_4\text{Ni}_3\text{O}_{10}$, the value of $1/T_1T$ at the La(1) site is much smaller than that at the La(2) site even at high temperatures, suggesting weaker hyperfine coupling with the Ni magnetic moments at La(1) site. Alternatively, in $\text{La}_4\text{Ni}_3\text{O}_{10}$, the magnetic moments of Ni in the middle layer may be oriented opposite to those in the outer layers[22], resulting in canceling contributions from the two Ni layers at the La(1) site and thus weaker magnetic fluctuations there.

In comparison with $\text{La}_3\text{Ni}_2\text{O}_7$ [15], we observe that $1/T_1T$ in $\text{La}_4\text{Ni}_3\text{O}_{10}$ retains a notable residual value, approximately 20% of its high-temperature value, even at the lowest temperature. In contrast, $1/T_1T$ in $\text{La}_3\text{Ni}_2\text{O}_7$ becomes negligibly small at the lowest temperature. These findings indicate that a substantial fraction of the Fermi surface remains ungapped in $\text{La}_4\text{Ni}_3\text{O}_{10}$, whereas it is nearly fully gapped in $\text{La}_3\text{Ni}_2\text{O}_7$. Furthermore, the DW order in $\text{La}_4\text{Ni}_3\text{O}_{10}$ is incommensurate, while it is commensurate in $\text{La}_3\text{Ni}_2\text{O}_7$. These observations suggest that the emergence of the DW in $\text{La}_4\text{Ni}_3\text{O}_{10}$ is closely related to Fermi surface nesting[40]. This nesting not only prevents the complete gapping of the Fermi surface but also gives rise to the incommensurate modulation of the DW orders. Additionally, previous theoretical studies have demonstrated that interlayer coupling plays a pivotal role in the emergence of antiferromagnetism and superconductivity in $\text{La}_4\text{Ni}_3\text{O}_{10}$ [41–43]. Specifically, this could explain why the Ni atoms on the outer planes exhibit a much larger magnetic moment in $\text{La}_4\text{Ni}_3\text{O}_{10}$, yet T_{SDW} is lower compared to that of $\text{La}_3\text{Ni}_2\text{O}_7$.

IV. CONCLUSION

In summary, our ^{139}La NQR measurements have revealed key microscopic insights into the intertwined CDW and SDW orders in $\text{La}_4\text{Ni}_3\text{O}_{10}$ at ambient pressure. Below $T_{\text{DW}} \approx 133$ K, the abrupt broadening and frequency shift of the NQR lines provide compelling evidence for a first-order-like DW transition. The pronounced broadening of the NQR spectra indicates the incommensurate nature of the DW order. Furthermore, the $1/T_1T$ exhibits a strong enhancement at T_{DW} , signifying the strong spin fluctuations originate from the SDW. While the sudden change of the spectra suggests that the first-order transition might be primarily driven by the CDW, highlighting a complex interplay between the CDW and SDW orders. Our findings not only elucidate the microscopic mechanisms underlying the DW state in $\text{La}_4\text{Ni}_3\text{O}_{10}$ but also provide a crucial framework for understanding the interplay between DW and superconducting phases in nickelate superconductors.

Acknowledgments

This work was supported by the National Key Research and Development Projects of China (Grants No. 2023YFA1406103, No. 2024YFA1611302, No. 2024YFA1409200 and No. 2022YFA1403402), the National Natural Science Foundation of China (Grants No. 12374142, No. 12304170 and No. U23A6003), Beijing National Laboratory for Condensed Matter Physics (Grant No. 2024BNLCMPKF005), the CAS Superconducting Research Project under Grant No. [SCZX-01011] and the Science and Technology Commission of Shanghai Municipality (No. 25DZ3008200). J.Z. was supported by the National Natural Science Foundation of China (Grants Nos. 12074219 and 12374457). This work was supported by the Synergetic Extreme Condition User Facility (SECUF, <https://cstr.cn/31123.02.SECUF>).

DATA AVAILABILITY

The data that support the finding of this article are not publicly available. The data are available from the authors upon reasonable request.

- [1] H. L. Sun, M. W. Huo, X. W. Hu, J. Y. Li, Z. J. Liu, Y. F. Han, L. Y. Tang, Z. Q. Mao, P. T. Yang, B. Wang, J. G. Cheng, D. X. Yao, G. M. Zhang and M. Wang, Signatures of superconductivity near 80 K in a nickelate under high pressure, [Nature 621, 493–498 \(2023\)](#).
- [2] N. N. Wang, G. Wang, X. L. Shen, J. Hou, J. Luo, X. P. Ma, H. X. Yang, L. F. Shi, J. Dou, J. Feng, J. Yang, Y. Q. Shi, Z. Ren, H. Ma, P. T. Yang, Z. Y. Liu, Y. Liu, H. Zhang, X. L. Dong, Y. X. Wang, K. Jiang, J. P. Hu, S. Nagasaki, K. Kitagawa, S. Calder, J. Q. Yan, J. P. Sun, B. Wang, R. Zhou, Y. Uwatoko and J. G. Cheng, Bulk high-temperature superconductivity in pressurized tetragonal $\text{La}_2\text{PrNi}_2\text{O}_7$, [Nature 634, 579–584 \(2024\)](#).
- [3] F. Y. Li, Z. F. Xing, D. Peng, J. Dou, N. Guo, L. Ma, Y. L. Zhang, L. Z. Wang, J. Luo, J. Yang, J. Zhang, T. Y. Chang, Y. S. Chen, W. Cai, J. G. Cheng, Y. Z. Wang, Z. D. Zeng, Q. Zheng, R. Zhou, Q. S. Zeng, X. T. Tao and J. J. Zhang, Ambient pressure growth of bilayer nickelate single crystals with superconductivity over 90 K under high pressure, [arXiv:2501.14584 \(2025\)](#).
- [4] Y. H. Zhu, D. Peng, E. K. Zhang, B. Y. Pan, X. Chen, L. X. Chen, H. F. Ren, F. Y. Liu, Y. Q. Hao, N. N. Li, Z. F. Xing, F. J. Lan, J. Y. Han, J. J. Wang, D. H. Jia, H. J. Wo, Y. Q. Gu, Y. M. Gu, L. Ji, W. B. Wang, H. Y. Gou, Y. Shen, T. P. Ying, X. L. Chen, W. G. Yang, H. B. Cao, C. L. Zheng, Q. S. Zeng, J. G. Guo and J. Zhao, Superconductivity in pressurized trilayer $\text{La}_4\text{Ni}_3\text{O}_{10-\delta}$ single crystals, [Nature 631, 531–536 \(2024\)](#).
- [5] Q. Li, Y. J. Zhang, Z. N. Xiang, Y. H. Zhang, X. Y. Zhu and H. H. Wen, Signature of Superconductivity in Pressurized $\text{La}_4\text{Ni}_3\text{O}_{10}$, [Chin. Phys. Lett. 41, 017401 \(2024\)](#).
- [6] M. X. Zhang, C. Y. Pei, D. Peng, X. Du, W. X. Hu, Y. T. Cao, Q. Wang, J. F. Wu, Y. D. Li, H. Y. Liu, C. H. P. Wen, J. Song, Y. Zhao, C. H. Li, W. Z. Cao, S. H. Zhu, Q. Zhang, N. Yu, P. H. Cheng, L. L. Zhang, Z. W. Li, J. K. Zhao, Y. L. Chen, C. Q. Jin, H. J. Guo, C. J. Wu, F. Yang, Q. S. Zeng, S. C. Yan, L. X. Yang and Y. P. Qi, Superconductivity in Trilayer Nickelate $\text{La}_4\text{Ni}_3\text{O}_{10}$ under Pressure, [Phys. Rev. X 15, 021005 \(2025\)](#).
- [7] F. Y. Li, Y. Q. Hao, N. Guo, D. H. Jia, J. Dou, D. Peng, G. T. Zhang, L. F. Xiao, J. Zhang, W. J. Zhou,

Y. H. Huang, X. Y. Wang, Z. Y. Guo, M. Mezouar, J. E. F. S. Rodrigues, J. Luo, J. Yang, Q. S. Zeng, R. Zhou, H. Y. Gou, Q. Zheng, G. T. Liu and J. J. Zhang, Single-Crystal Structure Determination of Superconducting $\text{La}_4\text{Ni}_3\text{O}_{10-\delta}$ under High Pressure, *Adv. Mater.* **37**, e07365 (2024).

[8] R. A. Mohan Ram, L. Ganapathi, P. Ganguly and C. N. R. Rao, Evolution of three-dimensional character across the $\text{La}_{n+1}\text{Ni}_n\text{O}_{3n+1}$ homologous series with increase in n, *J. Solid State Chem.* **63**(2), 139–147 (1986).

[9] K. Sreedhar, M. McElfresh, D. Perry, D. Kim, P. Metcalf and J. M. Honig, Low-Temperature Electronic Properties of the $\text{La}_{n+1}\text{Ni}_n\text{O}_{3n+1}$ (n = 2, 3, and ∞) System: Evidence for a Crossover from Fluctuating-Valence to Fermi-Liquid-like Behavior, *J. Solid State Chem.* **110**(2), 208–215 (1994).

[10] Y. Kobayashi, S. Taniguchi, M. Kasai, M. Sato, T. Nishioka and M. Kontani, Transport and Magnetic Properties of $\text{La}_3\text{Ni}_2\text{O}_{7-\delta}$ and $\text{La}_4\text{Ni}_3\text{O}_{10-\delta}$, *J. Phys. Soc. Jpn.* **65**, 3978–3982 (1996).

[11] G. Q. Wu, J. J. Neumeier and M. F. Hundley, Magnetic susceptibility, heat capacity, and pressure dependence of the electrical resistivity of $\text{La}_3\text{Ni}_2\text{O}_7$ and $\text{La}_4\text{Ni}_3\text{O}_{10}$, *Phys. Rev. B* **63**, 245120 (2001).

[12] K. W. Chen, X. Q. Liu, J. C. Jiao, M. Y. Zou, C. Y. Jiang, X. Li, Y. X. Luo, Q. Wu, N. Y. Zhang, Y. F. Guo and L. Shu, Evidence of Spin Density Waves in $\text{La}_3\text{Ni}_2\text{O}_{7-\delta}$, *Phys. Rev. Lett.* **132**, 256503 (2024).

[13] X. Y. Chen, J. W. Choi, Z. C. Jiang, J. Mei, K. Jiang, J. Li, S. Agrestini, M. Garcia-Fernandez, H. L. Sun, X. Huang, D. W. Shen, M. Wang, J. P. Hu, Y. Lu, K. J. Zhou and D. L. Feng, Electronic and magnetic excitations in $\text{La}_3\text{Ni}_2\text{O}_7$, *Nat. Commun.* **15**, 9597 (2024).

[14] D. Zhao, Y. B. Zhou, M. W. Huo, Y. Wang, L. P. Nie, Y. Yang, J. J. Ying, M. Wang, T. Wu and X. H. Chen, Pressure-enhanced spin-density-wave transition in double-layer nickelate $\text{La}_3\text{Ni}_2\text{O}_{7-\delta}$, *Sci. Bull.* **70**, 1239-1245 (2025).

[15] J. Luo, J. Feng, G. Wang, N. N. Wang, J. Dou, A. F. Fang, J. Yang, J. G. Cheng, G. Zheng and R. Zhou, Microscopic evidence of charge- and spin-density waves in $\text{La}_3\text{Ni}_2\text{O}_{7-\delta}$ revealed by ^{139}La -NQR, *Chin. Phys. Lett.* **42**(6), 067402 (2025).

[16] B. Keimer, S. A. Kivelson, M. R. Norman, S. Uchida and J. Zaanen, From quantum matter to high-temperature superconductivity in copper oxides, *Nature* **518**, 179-186 (2015).

[17] J. Paglione and R. L. Greene, High-temperature superconductivity in iron-based materials, *Nat. Phys.* **6**, 645-658 (2010).

[18] H. X. Li, X. Q. Zhou, T. Nummy, J. J. Zhang, V. Pardo, W. E. Pickett, J. F. Mitchell and D. S. Dessau, Fermiology and electron dynamics of trilayer nickelate $\text{La}_4\text{Ni}_3\text{O}_{10}$, *Nat. Commun.* **8**, 704 (2017).

[19] J. Y. Li, C. Q. Chen, C. X. Huang, Y. F. Han, M. W. Huo, X. Huang, P. Y. Ma, Z. Y. Qiu, J. F. Chen, X. W. Hu, L. Chen, T. Xie, B. Shen, H. L. Sun, D. X. Yao and M. Wang, Structural transition, electric transport, and electronic structures in the compressed trilayer nickelate $\text{La}_4\text{Ni}_3\text{O}_{10}$, *Sci. China Phys. Mech. Astron.* **67**, 117403 (2024).

[20] I. V. Leonov, Electronic structure and magnetic correlations in the trilayer nickelate superconductor $\text{La}_4\text{Ni}_3\text{O}_{10}$ under pressure, *Phys. Rev. B* **109**, 235123 (2024).

[21] Y. X. Wang, K. Jiang, Z. Q. Wang, F. C. Zhang and J. P. Hu, Electronic and magnetic structures of bilayer $\text{La}_3\text{Ni}_2\text{O}_7$ at ambient pressure, *Phys. Rev. B* **110**, 205122 (2024).

[22] H. LaBollita, J. Kapeghian, M. R. Norman and A. S. Botana, Electronic structure and magnetic tendencies of trilayer $\text{La}_4\text{Ni}_3\text{O}_{10}$ under pressure: Structural transition, molecular orbitals, and layer differentiation, *Phys. Rev. B* **109**, 195151 (2024).

[23] J. J. Zhang, D. Phelan, A. S. Botana, Y.-S. Chen, H. Zheng, M. Krogstad, S. G. Wang, Y. M. Qiu, J. A. Rodriguez-Rivera, R. Osborn, S. Rosenkranz, M. R. Norman and J. F. Mitchell, Intertwined density waves in a metallic nickelate, *Nat. Commun.* **11**, 6003 (2020).

[24] Y. D. Li, Y. T. Cao, L. Y. Liu, P. Peng, H. Lin, C. Y. Pei, M. X. Zhang, H. Wu, X. Du, W. X. Zhao, K. Y. Zhai, X. F. Zhang, J. K. Zhao, M. L. Lin, P. H. Tan, Y. P. Qi, G. Li, H. J. Guo, L. Y. Yang and L. X. Yang, Distinct ultrafast dynamics of bilayer and trilayer nickelate superconductors regarding the density-wave-like transitions, *Sci. Bull.* **70**(2), 180–186 (2025).

[25] S. X. Xu, C. Q. Chen, M. W. Huo, D. Y. Hu, H. Wang, Q. Wu, R. S. Li, D. Wu, M. Wang, D. X. Yao, T. Dong and N. L. Wang, Origin of the density wave instability in trilayer nickelate $\text{La}_4\text{Ni}_3\text{O}_{10}$ revealed by optical and ultrafast spectroscopy, *Phys. Rev. B* **111**, 075140 (2025).

[26] S. X. Xu, H. Wang, M. W. Huo, D. Y. Hu, Q. Wu, L. Yue, D. Wu, M. Wang, T. Dong and N. L. Wang, Collapse of density wave and emergence of superconductivity in pressurized- $\text{La}_4\text{Ni}_3\text{O}_{10}$ evidenced by ultrafast spectroscopy, *Nat. Commun.* **16**, 7039 (2025).

[27] M. Z. Li, J. S. Gong, Y. H. Zhu, Z. Y. Chen, J. K. Zhang, E. K. Zhang, Y. J. Li, R. T. Yin, S. Y. Wang, J. Zhao, D. L. Feng, Z. Y. Du and Y. J. Yan, Direct Visualization of an Incommensurate Unidirectional Charge Density Wave in $\text{La}_4\text{Ni}_3\text{O}_{10}$, *Phys. Rev. B* **112**, 045132 (2025).

[28] Y. T. Cao, A. Liu, B. Wang, M. X. Zhang, Y. P. Qi, T. J. Hicken, H. Luetkens, Z. D. Fu, J. S. Gardner, J. K. Zhao and H. J. Guo, Complex spin density wave ordering in $\text{La}_4\text{Ni}_3\text{O}_{10}$, *Phys. Rev. B* (2025).

[29] R. Khasanov, T. J. Hicken, I. Plokhikh, V. Sazgari, L. Keller, V. Pomjakushin, M. Bartkowiak, S. Królak, M. J. Winiarski, J. A. Krieger, H. Luetkens, T. Klimczuk, D. J. Gawryluk and Z. Guguchia,

Identical Suppression of Spin and Charge Density Wave Transitions in $\text{La}_4\text{Ni}_3\text{O}_{10}$ by Pressure, [arXiv:2503.04400](https://arxiv.org/abs/2503.04400) (2025).

- [30] T. Fukamachi, K. Oda, Y. Kobayashi, T. Miyashita and M. Sato, Studies on Successive Electronic State Changes in Systems with NiO_2 Planes – ^{139}La -NMR/NQR–, *J. Phys. Soc. Jpn.* **70**, 2757–2764 (2001).
- [31] M. Kakoi, T. Oi, Y. Ohshita, M. Yashima, K. Kuroki, T. Kato, H. Takahashi, S. Ishiwata, Y. Adachi, N. Hatada, T. Uda and H. Mukuda, Multiband Metallic Ground State in Multilayered Nickelates $\text{La}_3\text{Ni}_2\text{O}_7$ and $\text{La}_4\text{Ni}_3\text{O}_{10}$ Probed by ^{139}La -NMR at Ambient Pressure, *J. Phys. Soc. Jpn.* **93**, 053702 (2024).
- [32] M. X. Zhang, C. Y. Pei, Q. Wang, Y. Zhao, C. H. Li, W. Z. Cao, S. H. Zhu, J. F. Wu and Y. P. Qi, Effects of pressure and doping on Ruddlesden-Popper phases $\text{La}_{n+1}\text{Ni}_n\text{O}_{3n+1}$, *J. Mater. Sci. Technol.* **185**, 147–154 (2024).
- [33] F. Y. Li, S. L. Wang, C. Ma, X. L. Wang, C. Liu, C. Y. Fan, L. Han, S. P. Wang, X. T. Tao and J. J. Zhang, Flux Growth of Trilayer $\text{La}_4\text{Ni}_3\text{O}_{10}$ Single Crystals at Ambient Pressure, *Cryst. Growth Des.* **24(1)**, 347–354 (2024).
- [34] J. Chepin and J. H. Ross Jr., Magnetic spin-lattice relaxation in nuclear quadrupole resonance: the $\eta \neq 0$ case, *J. Phys.: Condens. Matter* **3**, 8103 (1991).
- [35] R. Blinc and T. Apih, NMR in multidimensionally modulated incommensurate and CDW systems, *Prog. Nucl. Magn. Reson. Spectrosc.* **41(1-2)**, 49–82 (2002).
- [36] Z. Li, R. Zhou, Y. Liu, D. L. Sun, J. Yang, C. T. Lin and G. Q. Zheng, Microscopic coexistence of antiferromagnetic order and superconductivity in $\text{Ba}_{0.77}\text{K}_{0.23}\text{Fe}_2\text{As}_2$, *Phys. Rev. B* **86**, 180501(R) (2012).
- [37] M. R. Norman, Landau theory of the density wave transition in trilayer Ruddlesden-Popper nickelates, *Phys. Rev. B* **112**, 075149 (2025).
- [38] J. Luo, Z. Zhao, Y. Z. Zhou, J. Yang, A. F. Fang, H. T. Yang, H. J. Gao, R. Zhou and G. Q. Zheng, Possible star-of-David pattern charge density wave with additional modulation in the kagome superconductor CsV_3Sb_5 , *npj Quantum Mater.* **7**, 30 (2022).
- [39] X. Y. Feng, Z. Zhao, J. Luo, J. Yang, A. F. Fang, H. T. Yang, H. J. Gao, R. Zhou and G. Q. Zheng, Commensurate-to-incommensurate transition of charge-density-wave order and a possible quantum critical point in pressurized kagome metal CsV_3Sb_5 , *npj Quantum Mater.* **8**, 23 (2023).
- [40] X. Du, Y. L. Wang, Y. D. Li, Y. T. Cao, M. X. Zhang, C. Y. Pei, J. M. Yang, W. X. Zhao, K. Y. Zhai,

Z. K. Liu, Z. W. Li, J. K. Zhao, Z. T. Liu, D. W. Shen, Z. Li, Y. He, Y. L. Chen, Y. P. Qi, H. J. Guo and L. X. Yang, Dichotomy in Low- and High-Energy Band Renormalizations in Trilayer Nickelate $\text{La}_4\text{Ni}_3\text{O}_{10}$: A Comparison with Cuprates, [Phys. Rev. Lett. **135**, 146506 \(2025\)](#).

[41] Z. H. Huo, P. Zhang, Z. H. Zhang, D. F. Duan and T. Cui, Electronic correlations and Hund's rule coupling in trilayer nickelate $\text{La}_4\text{Ni}_3\text{O}_{10}$, [Sci. China Phys. Mech. Astron. **68**, 127411 \(2025\)](#).

[42] P. F. Tian, H. T. Ma, X. Ming, X. J. Zheng and H. Li, Effective model and electron correlations in trilayer nickelate superconductor $\text{La}_4\text{Ni}_3\text{O}_{10}$, [J. Phys. Condens. Matter **36**, 355602 \(2024\)](#).

[43] Q. G. Yang, K. Y. Jiang, D. Wang, H. Y. Lu and Q. H. Wang, Effective model and s_{\pm} -wave superconductivity in trilayer nickelate $\text{La}_4\text{Ni}_3\text{O}_{10}$, [Phys. Rev. B **109**, L220506 \(2024\)](#).